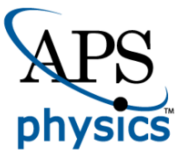

Topological Phononic Crystals with One-Way Elastic Edge Waves

Pai Wang, Ling Lu, and Katia Bertoldi

Phys. Rev. Lett. **115**, 104302 — Published 4 September 2015

DOI: 10.1103/PhysRevLett.115.104302

Topological Phononic Crystals with One-Way Elastic Edge Waves

Pai Wang,[1] Ling Lu,[2] and Katia Bertoldi[1,3,*]

[1]*Harvard John A. Paulson School of Engineering and Applied Sciences, Harvard University, Cambridge, Massachusetts 02138, USA*
[2]*Department of Physics, MIT, Cambridge, Massachusetts 02139, USA*
[3]*Kavli Institute, Harvard University, Cambridge, Massachusetts 02138, USA*

(Dated: 10th August 2015)

We report a new type of phononic crystals with topologically non-trivial bandgaps for both longitudinal and transverse polarizations, resulting in protected one-way elastic edge waves. In our design, gyroscopic inertial effects are used to break the time-reversal symmetry and realize the phononic analogue of the electronic quantum (anomalous) Hall effect. We investigate the response of both hexagonal and square gyroscopic lattices and observe bulk Chern number of 1 and 2, indicating that these structures support single and multi-mode edge elastic waves immune to back-scattering. These robust one-way phononic waveguides could potentially lead to the design of a novel class of surface wave devices that are widely used in electronics, telecommunication and acoustic imaging.

Topological states in electronic materials, including the quantum Hall effect [1] and topological insulators [2, 3], have inspired a number of recent developments in photonics [4, 5], phononics [6–9] and mechanical metamaterials [10–13]. In particular, in analogy to the quantum anomalous Hall effect [14], one-way electromagnetic waveguides in two-dimensional systems have been realized by breaking time-reversal symmetry [15–18].

Very recently unidirectional edge channels have been proposed for elastic waves by Coriolis force in a non-inertial reference frame [19], but such a rotating frame is very difficult to be implemented in solid state devices. Moreover, one-way propagation of scalar acoustic waves has also been proposed by introducing rotating fluids [20, 21]. However, it is important to recognize that elastic waves in solids have both transverse and longitudinal polarizations, while acoustic waves in fluids are purely longitudinal. As a result, it is challenging to achieve topological protection for elastic waves in an integrated device platform.

Here, we present a robust strategy to create topologically nontrivial edge modes for both longitudinal and transverse polarizations in a solid medium. In particular, we introduce gyroscopic phononic crystals, where each lattice site is coupled with a spinning gyroscope that breaks time-reversal symmetry in a well-controlled manner. In both hexagonal and square lattices, gyroscopic coupling opens bandgaps that are characterized by Chern numbers of 1 and 2. As a result, at the edge of these lattices both single-mode and multi-mode one-way elastic waves are observed to propagate around arbitrary defects without backscattering.

To start, we consider a hexagonal phononic crystal with equal masses ($m_2 = m_1$) connected by linear springs (red and black rods in Figs. 1a and 1b). The resulting unit cell has four degrees of freedom specified by the displacements of m_1 and m_2 ($\mathbf{U} = [u_x^{m_1}, u_y^{m_1}, u_x^{m_2}, u_y^{m_2}]$). Consequently, there are a total of four bands in the band structure (Fig. 1c). Note that this is the minimal number of bands required to open a complete bandgap, since the first two elastic dispersions are pinned at zero frequency. The phononic band structures are calculated by solving the dispersion equation [22]

$$\left[\mathbf{K}(\boldsymbol{\mu}) - \omega^2\mathbf{M}\right]\mathbf{U} = \mathbf{0} \tag{1}$$

for wave vectors $\boldsymbol{\mu}$ within the first Brillouin zone. Here, ω denotes the angular frequency of the propagating wave and $\mathbf{M} = \mathrm{diag}\{m_1, m_1, m_2, m_2\}$ is the mass matrix. Moreover, $\mathbf{K}$ is the 4×4 stiffness matrix and is a function of the Bloch wave vector $\boldsymbol{\mu}$. The band structure of this simple lattice is shown in Fig. 1c. As expected, in the long wavelength regime (near G-point) the first and second bands correspond to transverse and longitudinal modes, respectively, while for short wavelengths (near K-points) all modes are found to have mixed polarization (detailed analysis of the modal polarization is given in Supplementary Materials [23]). Moreover, we observe a quadratic degeneracy between the third and fourth bands at the center of the Brillouin zone and a complete gap between the second and third bands due to the lack of inversion symmetry. However, this gap is topologically trivial, since time-reversal symmetry is not broken and the Chern numbers of the bands are all zero.

In order to break time-reversal symmetry, we introduce gyroscopic coupling [24–26] and attach each mass in the lattice to the tip of the rotational axis of a gyroscope, as shown in Fig. 1d. Note that the other tip of the gyroscope is pinned to the ground to prevent any translational motion, while allowing for free rotations. Because of the small-amplitude in-plane waves propagating in the phononic lattice, the magnitude of the tip displacement of the each gyroscope is given by

$$U_{tip} = h\sin\theta \approx h\theta = h\Theta e^{i\omega t} \quad \text{for} \quad |\Theta| \ll 1, \tag{2}$$

where h and θ denote the height and nutation angle of the gyroscope (Fig. 1d) and Θ is the amplitude

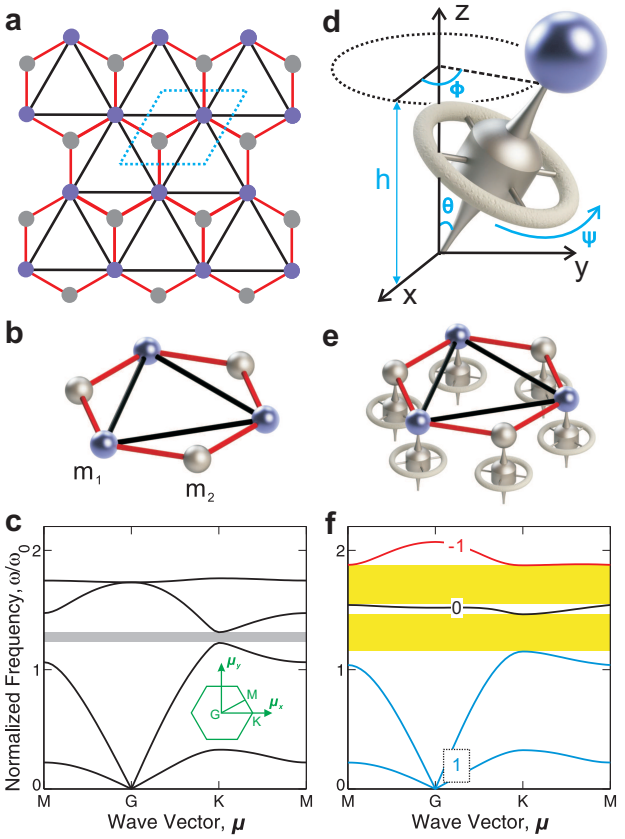

Figure 1: **Ordinary and Gyroscopic Phononic Crystals: (a)** Schematic of the hexagonal lattice. The blue and grey spheres represent concentrated masses m_1 and $m_2 = m_1$, respectively. The red and black straight rods represent mass-less linear springs with stiffness k_1 and $k_2 = k_1/20$, respectively. The dashed cell is the primitive cell of the lattice. **(b)** Unit cell for the ordinary (non-gyroscopic) phononic crystal. **(c)** Band structure of the ordinary (non-gyroscopic) phononic crystal. The inset is the Brillouin zone. **(d)** Schematic of a gyroscope with the top tip pinned to a mass in the lattice. **(e)** Unit cell for the gyroscopic phononic crystal. **(f)** Band structure of the gyroscopic phononic crystal ($\alpha_1 = \alpha_2 = 0.3m_1$) with the Chern numbers labeled on the bulk bands. The frequencies are normalized by $\omega_0 = \sqrt{k_1/m_1}$.

of the harmonic change in θ. Interestingly, the coupling between the mass in the lattice and the gyroscope induces an in-plane gyroscopic inertial force perpendicular to the direction of U_{tip} [23, 25, 27]:

$$F_g = \pm i\omega^2 \alpha U_{tip}, \tag{3}$$

where α is the spinner constant that characterizes the strength of the rotational coupling between two independent inertias in the 2D plane. As a result, the mass matrix in Eq. (1) becomes,

$$\tilde{\mathbf{M}} = \mathbf{M} + \begin{pmatrix} 0 & i\alpha_1 & 0 & 0 \\ -i\alpha_1 & 0 & 0 & 0 \\ 0 & 0 & 0 & i\alpha_2 \\ 0 & 0 & -i\alpha_2 & 0 \end{pmatrix}, \tag{4}$$

where α_1 and α_2 denote the spinner constants of the gyroscopes attached to m_1 and m_2, respectively. We note that the imaginary nature of the gyroscopic inertial effect indicates directional phase shifts with respect to the tip displacements, which breaks time-reversal symmetry.

We now consider the band structure of the gyroscopic hexagonal lattice. Interestingly, we find that the original bandgap between the second and third bands first closes into a Dirac cone at the K-points and then reopens as we gradually increase the magnitude of α_1 and α_2. In particular, for $\alpha_1 = \alpha_2 = 0.07m_1$ the gap is closed and a pair of Dirac cones at K-points emerges, while for $\alpha_1 = \alpha_2 = 0.3m_1$ the gap reopens, as shown in Fig. 1f. We also note that this topological transition at $\alpha_1 = \alpha_2 = 0.07m_1$ is accompanied by a band inversion [9] between the second and third bands near the K-points (the complete process of this topological transition is shown in the Supplementary Materials [23]). Since each Dirac point carries a Berry phase of π and there is a pair of Dirac cones in the first Brillouin zone [28], we expect the total exchange of Berry curvature between the two bands to be 2π, resulting in one chiral edge state in the gap between the second and third bands. Similarly, we also observe that the quadratic degeneracy found for the ordinary lattice between the third and fourth bands at the Brillouin zone center (see Fig. 1c) is opened into a full band gap when gyroscopic coupling is introduced (see Fig. 1f). Since such a quadratic touching carries a 2π Berry phase [29], there should be one chiral edge state in the gap between the third and fourth bands. Importantly, the fact that bandgaps in Fig. 1f are topologically-nontrivial is confirmed by the non-zero Chern numbers labeled on the bands (the calculations conducted to compute these topological invariants are detailed in the Supplementary Materials [23]). Therefore, in the frequency ranges of these nontrivial bandgaps, we expect gapless one-way edge states, whose number is dictated by the sum of Chern numbers below the bandgap, in agreement with our intuitive arguments of Berry phase.

To verify the existence of such one-way edge states, we perform one-dimensional (1D) Bloch wave analyses on a supercell comprising 20×1 unit cells, assuming free boundary conditions for the top and bottom edges. In full agreement with the bulk Chern numbers, the band structure of the supercell shows one one-way edge mode on each edge in both bandgaps. For modes bound to the top edge (Fig. 2b), the propagation can only assume negative group velocities (red solid lines with negative slope in Fig. 2a). On the other hand, the modes bound to the bottom edge (Fig. 2c) possess positive group velocities (blue dashed lines with positive slope in Fig. 2a). Since these edge modes are in the gap frequency range where no bulk modes may exist, they cannot scatter into the bulk of the phononic crystal. Furthermore, their uni-directional

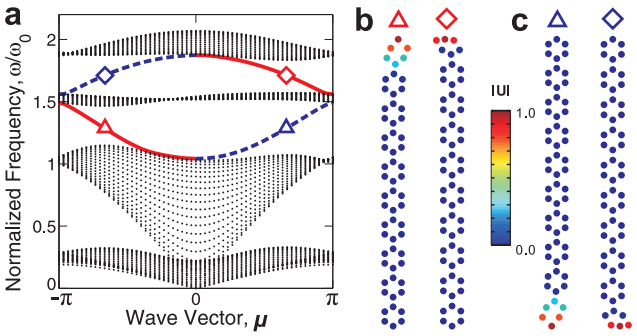

Figure 2: **Edge modes in Gyroscopic Phononic Crystal: (a)** 1D band structure showing bulk bands (black dots) and edge bands (colored lines). Red solid lines represent edge modes bound to the top boundary, while blue dashed lines represent edge modes bound to the bottom boundary. **(b)** Modal displacement fields of top edge states with negative group velocities. **(c)** Modal displacement fields of bottom edge states with positive group velocities

group velocities guarantee the absence of any back scattering and result in the topologically protected one-way propagation of vibration energy.

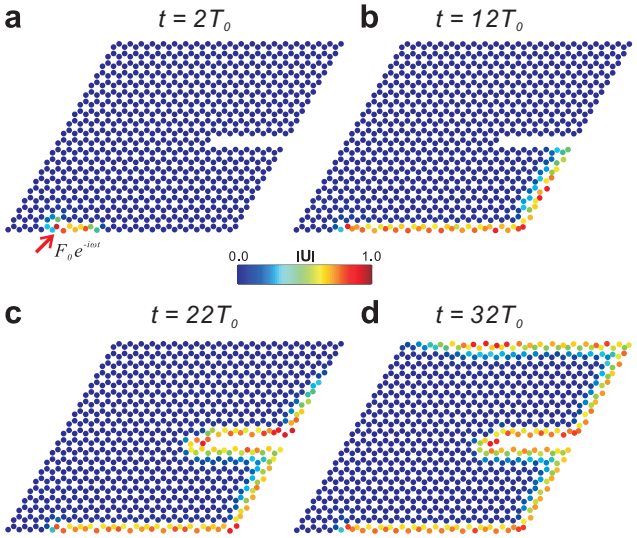

Figure 3: **Transient Response** of a gyroscopic phononic crystal consisting of 20 × 20 unit cells with a line defect on the right boundary: Snapshots of the displacement field at **(a)** $t = 2T_0$, **(b)** $t = 12T_0$, **(c)** $t = 22T_0$ and **(d)** $t = 32T_0$, where $T_0 = \sqrt{m_1/k_1}$ is the characteristic time scale of the system. Starting from $t = 0$, a time-harmonic excitation force $\mathbf{F}(t) = [F_x(t), F_y(t)] = [1, 1]F_0e^{-i\omega t}$ is prescribed at the site indicated by the red arrow.

To show the robustness of these edge states, we conduct transient analysis on a finite sample comprising 20×20 unit cells with a line defect on the right boundary created by removing twelve masses and the springs connected to them (Fig. 3a). A harmonic force excitation, $F_0\mathrm{e}^{-i\omega t}$, is prescribed at a mass site on the bottom boundary (red arrow in Fig. 3a) with frequency within the bulk bandgap between the second and third bands ($\omega/\omega_0 = 1.3$). In Fig. 3 we plot snapshots of the velocity field at different time instances, $t/T_0 =$ 2, 12, 22 and 32, where $T_0 = \sqrt{m_1/k_1}$ is the characteristic time scale of the system. Remarkably, because of their topological protection, the edge modes circumvent both the sharp corner and the line defect without any reflection. We note that, although the results presented in Fig. 3 are for an harmonic excitation with 45° inclination (i.e. $\mathbf{F}(t) = [F_x(t), F_y(t)] = [1, 1]F_0e^{-i\omega t}$), the one-way edge propagation are not affected by the direction of the applied force (additional results are included in the Supplementary Materials [23]).

Next, we investigate the effect of the lattice geometry and start with an ordinary square phononic crystal with masses m_1 connected by springs with elastic constant k_1. To make the lattice statically stable, we add an additional mass $m_2 = m_1$ at the center of each unit cell and connect it to its four adjacent m_1 masses by springs with elastic constant $k_2 = 2k_1$ (See Figs. 4a). The band structure for this lattice (shown in Fig. 4b) contains a pair of three-fold linear degeneracy among the first, second and third bands at the X points of the Brillouin zone. Note that this type of degeneracy, consisting of a locally flat band and a Dirac point, is known as the "accidental Dirac point" or "Dirac-like cones" [30, 31]. Interestingly, while previously this type of degeneracy usually occurs at the Brillouin center and has been found to be very sensitive to the system parameters, in our lattice it robustly appears at the X points when $m_1 = m_2$. Upon the introduction of gyroscopic inertial effects ($\alpha_1 = \alpha_2 = 0.3\,m_1$), these three-fold degenerate points are lifted and a gap is created between the second and third bands (Fig. 4c). The Chern numbers of the two bulk bands below the gap is two, predicting the existence of two topological edge states. The presence of multi- mode one-way elastic waves is consistent with the fact that the Berry phase associated with such a three-band degeneracy is 2π [32], resulting in a total exchange of Berry curvature of 4π when gapping two of these points in the Brillouin zone [33]. In Figs. 4d and 4e, we plot the band structure of the corresponding 20×1 supercell, highlighting the two one-way edge modes and their modal displacement fields.

To summarize, we demonstrated that gyroscopic phononic crystals can support topologically non-trivial gaps, within which the edge states are unidirectional and immune to back-scattering. The transient analysis confirmed that the propagation of such topological edge waves is robust against large defect and sharp corners. Moreover, we showed, for the first time, the multimode one-way states (Chern number = ±2) in phononic systems, opening more avenues for the design

of future topological waveguides and devices. While in this study we developed a comprehensive framework for the design and analysis of topological phononic crystals, we recently became aware of a parallel effort in which time-reversal symmetry breaking in a gyroscopic system has been experimentally demonstrated [34].

Finally, we note that phononic crystals [35, 36] and acoustic metamaterials [37–41] that enable manipulation and control of elastic waves have received significant interest in recent years [22, 42], not only because of their rich physics, but also for their broad range of applications [43–55]. Interestingly, the edge wave modes in phononic crystals are important in many scenarios [56–59], including vibration control [60] and acoustic imaging [51]. However, most of reported studies have focused on topologically trivial surface waves that can be easily scattered or localized by defects [56]. Therefore, the work reported here could open new avenues for the design of phononic devices with special properties and functionalities on edges, surfaces and interfaces.

This work has been supported by NSF through grants CMMI-1120724, CMMI-1149456 (CAREER) and the Materials Research Science and Engineering Center (DMR-1420570). K.B. acknowledges start-up funds from the Harvard School of Engineering and Applied Sciences and the support of the Kavli Institute and Wyss Institute at Harvard University. L.L. was supported in part by U.S.A.R.O. through the ISN under Contract No. W911NF-13-D-0001, in part by the MRSEC Program of the NSF under Award No. DMR-1419807 and in part by the MIT S3TEC EFRC of DOE under Grant No. DE-SC0001299. The authors are also grateful to Scott Skirlo, Timothy H. Hsieh and Dr. Filippo Casadei for ispirational discussions and to Dr. Farhad Javid and Xin You for their support with graphics.

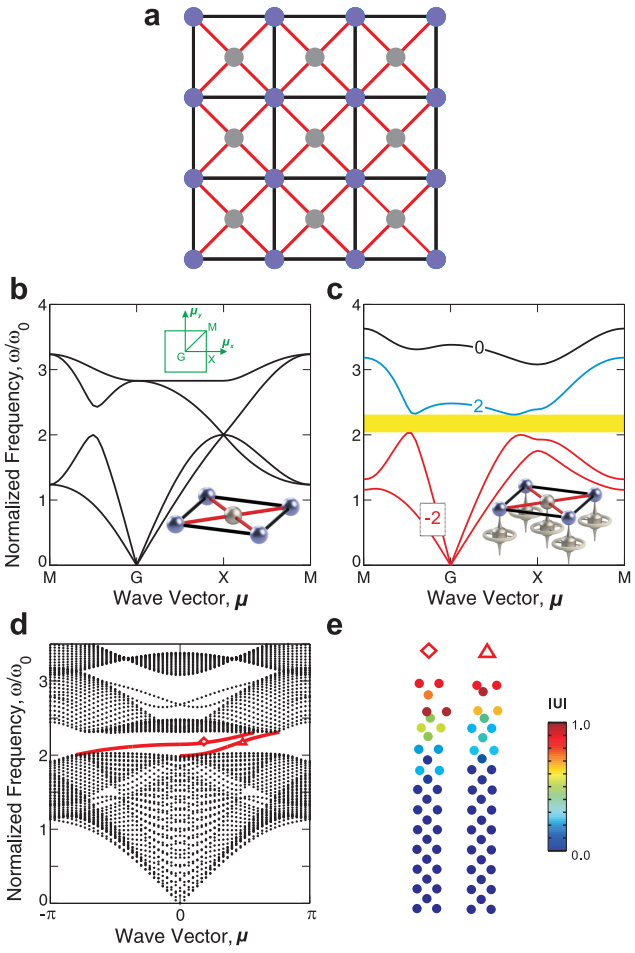

Figure 4: **Square Lattice results: (a)** Schematic of the square lattice. The blue and grey spheres represent concentrated masses m_1 and $m_2 = m_1$, respectively. The black and red straight rods represent mass-less linear springs with stiffness k_1 and $k_2 = 2k_1$, respectively. **(b)** Band structure of the ordinary (non-gyroscopic) phononic crystal. The insets are the Brillouin zone and the unit cell. **(c)** Band structure of the gyroscopic phononic crystal ($\alpha_1 = \alpha_2 = 0.3m_1$) with the Chern numbers labeled on the bulk bands. Frequencies are normalized by $\omega_0 = \sqrt{k_1/m_1}$. The inset is the unit cell. **(d)** 1D band structure showing bulk bands (black dots) and two topological edge bands (red solid lines) bound to the top boundary. Note that the edge bands that are bound to the bottom boundary are not shown here. **(e)** Modal displacement fields of the edge states shown in **(d)**.

* Corresponding author. bertoldi@seas.harvard.edu

[1] K. von Klitzing, Rev. Mod. Phys. **58**, 519 (1986).
[2] M. Z. Hasan and C. L. Kane, Rev. Mod. Phys. **82**, 3045 (2010).
[3] X.-L. Qi and S.-C. Zhang, Rev. Mod. Phys. **83**, 1057 (2011).
[4] F. D. M. Haldane and S. Raghu, Phys. Rev. Lett. **100**, 013904 (2008).
[5] L. Lu, J. D. Joannopoulos, and M. Soljačić, Nature Photonics (2014).
[6] E. Prodan and C. Prodan, Phys. Rev. Lett. **103**, 248101 (2009).
[7] L. Zhang, J. Ren, J.-S. Wang, and B. Li, Phys. Rev. Lett. **105**, 225901 (2010).
[8] R. Süsstrunk and S. D. Huber, arXiv preprint arXiv:1503.06808 (2015).
[9] M. Xiao, G. Ma, Z. Yang, P. Sheng, Z. Zhang, and C. Chan, Nature Physics (2015).
[10] K. Sun, A. Souslov, X. Mao, and T. Lubensky, Proceedings of the National Academy of Sciences **109**, 12369 (2012).
[11] C. Kane and T. Lubensky, Nature Physics **10**, 39 (2014).
[12] J. Paulose, B. G.-g. Chen, and V. Vitelli, Nature Physics (2015).
[13] B. G.-g. Chen, N. Upadhyaya, and V. Vitelli, Proceedings of the National Academy of Sciences **111**, 13004 (2014).
[14] F. D. M. Haldane, Phys. Rev. Lett. **61**, 2015 (1988).
[15] Z. Wang, Y. Chong, J. D. Joannopoulos, and M. Soljačić, Physical review letters **100**, 013905 (2008).
[16] Z. Wang, Y. Chong, J. Joannopoulos, and M. Soljačić,

Nature **461**, 772 (2009).
[17] S. A. Skirlo, L. Lu, and M. Soljačić, Physical Review Letters **113**, 113904 (2014).
[18] S. A. Skirlo, L. Lu, Y. Igarashi, J. Joannopoulos, and M. Soljacic, arXiv preprint arXiv:1504.04399 (2015).
[19] Y.-T. Wang, P.-G. Luan, and S. Zhang, arXiv preprint arXiv:1411.2806 (2014).
[20] R. Fleury, D. L. Sounas, C. F. Sieck, M. R. Haberman, and A. Alù, Science **343**, 516 (2014).
[21] Z. Yang, F. Gao, X. Shi, X. Lin, Z. Gao, Y. Chong, and B. Zhang, Phys. Rev. Lett. **114**, 114301 (2015).
[22] M. I. Hussein, M. J. Leamy, and M. Ruzzene, Applied Mechanics Reviews **66**, 040802 (2014).
[23] For additional results and detailed derivations and calculation procedures, see Supplementary Material at [URL], which includes References [9, 25–27, 61, 62].
[24] G. W. Milton and J. R. Willis, Proceedings of the Royal Society of London A: Mathematical, Physical and Engineering Sciences **463**, 855 (2007).
[25] M. Brun, I. S. Jones, and A. B. Movchan, Proceedings of the Royal Society of London A: Mathematical, Physical and Engineering Sciences **468**, 3027 (2012).
[26] G. Carta, M. Brun, A. Movchan, N. Movchan, and I. Jones, International Journal of Solids and Structures **51**, 2213 (2014).
[27] H. Goldstein, J. Safko, and C. Poole (2002).
[28] Note that on the boundary of the first Brillouin zone of the hexagonal lattice there are six Dirac points. However, since at each point only one third of the Dirac cone is included in the first Brillouin zone, we have a pair of Dirac cones in total.
[29] Y. Chong, X.-G. Wen, and M. Soljačić, Physical Review B **77**, 235125 (2008).
[30] F. Liu, X. Huang, and C. Chan, Applied Physics Letters **100**, 071911 (2012).
[31] X. Huang, Y. Lai, Z. H. Hang, H. Zheng, and C. Chan, Nature materials **10**, 582 (2011).
[32] J. Mei, Y. Wu, C. Chan, and Z.-Q. Zhang, Physical Review B **86**, 035141 (2012).
[33] Note that on the boundary of the first Brillouin zone of the square lattice there are four equivalent X-points. However, since at each point only one half of the three-band degeneracy is included in the first Brillouin zone, we have a pair of three-band degeneracies in total.
[34] L. M. Nash, D. Kleckner, A. Read, V. Vitelli, A. M. Turner, and W. T. Irvine, arXiv p. arXiv:1504.03362 (2015).
[35] M. Sigalas and E. Economou, Solid State Communications **86**, 141 (1993).
[36] M. S. Kushwaha, P. Halevi, L. Dobrzynski, and B. Djafari-Rouhani, Phys. Rev. Lett. **71**, 2022 (1993).
[37] Z. Liu, X. Zhang, Y. Mao, Y. Zhu, Z. Yang, C. Chan, and P. Sheng, Science **289**, 1734 (2000).
[38] N. Fang, D. Xi, J. Xu, M. Ambati, W. Srituravanich, C. Sun, and X. Zhang, Nature Materials **5**, 452 (2006).
[39] Y. Ding, Z. Liu, C. Qiu, and J. Shi, Phys. Rev. Lett. **99**, 093904 (2007).
[40] Y. Lai, Y. Wu, P. Sheng, and Z. Zhang, Nat. Mater. **10**, 620 (2011).
[41] P. Wang, F. Casadei, S. Shan, J. C. Weaver, and K. Bertoldi, Phys. Rev. Lett. **113**, 014301 (2014).
[42] M. Maldovan and E. Thomas, *Periodic Materials and Interference Lithography for Photonics, Phononics and Mechanics* (Wiley-VCH, 2009).
[43] M. Ruzzene, F. Scarpa, and F. Soranna, Smart. Mater. Struct. **12**, 363 (2003).
[44] S. Phani, J. Woodhouse, and N. A. Fleck, J. Acoust. Soc. Am. **119**, 1995 (2006).
[45] J. O. Vasseur, A. Hennion, B. Rouhani, F. Duval, B. Dubus, and Y. Pennec, J. App. Phys. **101**, 114904 (2007).
[46] M. Kafesaki, M. M. Sigalas, and N. Garcia, Phys. Rev. Lett. **85**, 4044 (2000).
[47] Y. Pennec, B. Djafari-Rouhani, J. O. Vasseur, A. Khelif, and P. A. Deymier, Phys. Rev. E **69**, 046608 (2004).
[48] J. Mei, G. Ma, M. Yang, Z. Yang, W. Wen, and P. Sheng, Nature Communications **3**, 756 (2012).
[49] S. Brûlé, E. H. Javelaud, S. Enoch, and S. Guenneau, Phys. Rev. Lett. **112**, 133901 (2014).
[50] L.-S. Chen, C.-H. Kuo, and Z. Ye, Applied Physics Letters **85**, 1072 (2004).
[51] J. Christensen, A. I. Fernandez-Dominguez, F. de Leon-Perez, L. Martin-Moreno, and F. J. Garcia-Vidal, Nat. Phys. **3**, 851 (2007).
[52] J. Li, L. Fok, X. Yin, G. Bartal, and X. Zhang, Nature materials **8**, 931 (2009).
[53] D. Bigoni, S. Guenneau, A. B. Movchan, and M. Brun, Phys. Rev. B **87**, 174303 (2013).
[54] M. Maldovan, Phys. Rev. Lett. **110**, 025902 (2013).
[55] B. L. Davis and M. I. Hussein, Phys. Rev. Lett. **112**, 055505 (2014).
[56] M. Torres, F. R. Montero de Espinosa, D. Garcia-Pablos, and N. Garcia, Phys. Rev. Lett. **82**, 3054 (1999).
[57] D. Torrent and J. Sánchez-Dehesa, Phys. Rev. Lett. **108**, 174301 (2012).
[58] N. Boechler, J. K. Eliason, A. Kumar, A. A. Maznev, K. A. Nelson, and N. Fang, Phys. Rev. Lett. **111**, 036103 (2013).
[59] Y. Li, Y. Wu, and J. Mei, Applied Physics Letters **105**, 014107 (2014).
[60] D. Torrent, D. Mayou, and J. Sánchez-Dehesa, Phys. Rev. B **87**, 115143 (2013).
[61] P. Wang and K. Bertoldi, *Towards phononic topological insulators*, Presented at APS March Meeting, A42.11 (2014).
[62] T. Fukui, Y. Hatsugai, and H. Suzuki, Journal of the Physical Society of Japan **74**, 1674 (2005).